Ergodic and nonergodic phases in a one-dimensional clean Jaynes-Cummings-Hubbard system with detuning

Jin-Lou Ma [1], Qing Li [1], and Lei Tan [1,2,*]

[1] *Lanzhou Center for Theoretical Physics, Key Laboratory of Theoretical Physics of Gansu Province, Lanzhou University, Lanzhou, Gansu 730000, China*

[2] *Key Laboratory for Magnetism and Magnetic Materials of the Ministry of Education, Lanzhou University, Lanzhou 730000, China*

(Received 13 December 2021; revised 23 April 2022; accepted 25 April 2022; published 29 April 2022)

We study the ergodic and nonergodic behaviors of a clean Jaynes-Cummings-Hubbard chain for different parameters based on the average level spacing ratios and the generalized fractal dimensions of eigenstates by using exact diagonalization. It can be found that a transition from ergodic to nonergodic regimes happens when increasing the atom-photon detuning, and the nonergodic phases should exist in the thermodynamic limit. We also find that the nonergodic phase violates the eigenstate thermalization hypothesis and displays many-body-localization-like behavior. Finally, we study the many-body multifractality of the ground state and find that the derivative of the generalized fractal dimensions can determine the critical point of the superfluid-Mott-insulation phase transition in a small range of parameters under different boundary conditions and there is no ergodicity for the ground state.

DOI: 10.1103/PhysRevB.105.165432

I. INTRODUCTION

Generally speaking, ergodicity is the basic hypothesis of classical statistical physics, which means that the system will visit each region of phase space in the process of time evolution and the time spent is proportional to the volume of the region under the long-time limit [1–3]. Learning from the idea of classical statistical mechanics, how to connect quantum mechanics with statistical physics has become a topic of interest. Based on Berry-Tabor conjecture [4], quantum ergodic theory comes into being: for any quantum system, it is assumed that the eigenstate of an ergodic Hamiltonian is essentially an uncorrelated random variable [5]. Therefore, using the random matrix theory (RMT), the eigenvalues and eigenstates of many-body quantum systems can predict the existence of ergodicity [3,6–11].

It was realized very early that not all systems are ergodic, in general, quantum integrable systems are nonergodic. When a generic perturbation is added, a few quantum integrable systems are unstable and become ergodic [5]. Ergodicity is an obvious property of quantum nonintegrable systems, but ergodicity breaking has been found in many cases due to different factors. For example, for a classical periodic driven one degree of freedom [11] or many-body systems [12–15], under the quantum regime, the interference effect leads to an inhibition of energy absorption and forms dynamic localization, which shows a nonergodic behavior. When a disorder is introduced, a complex many-body system cannot be thermalized and produces a spatially localized motion integral with a nonergodic behavior [16–20]. The ergodicity breaking also occurs in an incompletely chaotic nonintegrable system which keeps a memory of the initial state [21]. Since 2017, researchers have found that in lattice gauge theories, the emergence of local constraints leads to nonergodicity [22–28]. Later, it was found that the large tilt potential can also produce a similar effect to the disorder, resulting in the nonergodic many-body systems [29–32], which has been realized in the latest experiments [33,34]. In addition, the existence of nonergodic behaviors is also found for a one-dimensional uniform Josephson junction chain at higher energies or weak Josephson coupling [35] and a clean Bose-Hubbard chain under weak tunneling strength [36]. Interesting questions thus arise and need to be clarified, e.g., whether there are other factors that can lead to the ergodicity breaking?

Based on the above works, we are interested in exploring whether a clean Jaynes-Cummings-Hubbard (JCH) has a nonergodicity under the thermodynamic limit and whether the transition from ergodic to nonergodic phase can be controlled by changing the atom-photon detunings. In the study of ergodicity and nonergodicity of many-body systems mentioned above, most researchers mainly focus on spin, fermion, or boson systems with direct two-body interaction. While for the JCH model described a boson and spinlike hybrid system, only relatively fewer investigations on the ergodicity and thermalization are conducted. Recently, the eigenstate thermalization and quantum chaos of the JCH model are discussed primarily by our group based on the open boundary conditions for the resonance cases. It can be found that the JCH model has the property of the quantum chaotic system due to the competition between the effective on-site repulsive potential and the photon tunneling strength [37,38]. Significantly, the influence of the atom-photon detuning is absent. As is well known, detuning is an important controlled parameter, which is known to have a variety of practical consequences. A large number of novel physics emerging from the detuning has been widely explored, which includes the photon blockade [39], non-Markovian behavior [40], polariton Mott

*tanlei@lzu.edu.cn

 ©2022 American Physical Society

phases [41], geometric quantum computation [42], population transfer [43], and the modification of molecular spectra with detunings [44], *et al.* Physically, detuning can affect the properties of eigenenergies and eigenstates of the system by controlling the coupling between the atom and the cavity field, then the on-site repulsive potential can be regulated and the ergodicity may be changed correspondingly.

Inspired by these works, in this paper, we focus on the nonergodic and ergodic phase of a one-dimensional JCH model for small atom-photon detunings under almost all ranges of tunneling strength based on the average level spacing ratios and the finite-size generalized fractal dimensions (GFDs) in the periodic boundary condition (PBC). We first find that the atom-photon detuning can control the ergodic and nonergodic phases transition of the JCH model. With the increase of the absolute value of atom-photon detuning, the ergodic region of the system gradually decreases and then disappears. In the case of a atom-photon detuning, through finite-size analysis, it is predicted that ergodic breaking also exists under the thermodynamic limit. Then, through the eigenstate thermalization hypothesis (ETH), we further know that the nonergodic phase does not satisfy the thermalization behavior, which is similar to many-body localization and no corresponding single-particle similar phenomenon. It is very meaningful to the system that cannot be thermalized. In a such case, the information of the initial state can persist, and the dynamic behavior can be controlled under long-term evolution [20]. In addition, the positive and negative atom-photon detuning have different effects on the ground state ergodicity. Under the exact diagonalization, it is found that the critical phase transition point of superfluid (SF) to Mott insulation (MI) can be easily determined in a very small range of parameters by the derivative of GFDs.

The paper is organized as follows: In Sec. II the theoretical model is introduced, and we describe the required physical quantities and analyze the energy spectrum phase in Sec. III. Section IV is devoted to providing the relationship between the ground state phase transition and multifractal. The conclusions are summarized in Sec. V.

II. THEORETICAL MODEL

We study a one-dimensional JCH model including an atom-photon interaction term and a photon tunneling term between nearest neighboring cavities [45–47]. Using the rotating transformation operator $U = \exp[-i\sum_{j=1}^{L}\omega_c(a_j^\dagger a_j + \sigma_j^+\sigma_j^-)t]$, a generic Hamiltonian of the JCH model

$$H_{\rm gen} = \sum_i^L [\omega_c a_i^\dagger a_i + \omega_a \sigma_i^+\sigma_i^- + g_a(a_i\sigma_i^+ + a_i^\dagger\sigma_i^-)] - J\sum_i^L (a_i^\dagger a_{i+1} + a_i a_{i+1}^\dagger) \tag{2.1}$$

can be written as

$$H = H_{\rm int} + H_{\rm tun} = \sum_i^L [\Delta\sigma_i^+\sigma_i^- + g_a(a_i\sigma_i^+ + a_i^\dagger\sigma_i^-)] - J\sum_i^L (a_i^\dagger a_{i+1} + a_i a_{i+1}^\dagger), \tag{2.2}$$

where $\Delta = \omega_a - \omega_c$ is the atom-photon detuning, ω_a is the transition energy of the two-level atom in every cavity, and ω_c is the frequency of each cavity field. σ_i^+ and σ_i^- are the atomic raising and lowering operators, respectively. The second term of the local interaction Hamiltonian term $H_{\rm int}$ describes the on-site coupling between the photons and the atom on each site, and $a_i^\dagger$ (a_i) is the photonic creation (annihilation) operator in the ith site. We assume that all the atoms couple to cavities with the same coupling g_a. The tunneling Hamiltonian term $H_{\rm tun}$ is the sum of tunneling of photons and J is the hopping energy of photons between the nearest neighboring cavities i and $i+1$ for all cavities.

The JCH model is a typical model in the field of many-body quantum optics, which can be realized in superconducting circuit and traditional optical coupled-cavity arrays, respectively [48–50]. The relationships between the physical parameters studied on these two experimental platforms can be the same for the Hamiltonian Eq. (2.2). In general, atom-photon coupling strength $g_a \sim \sqrt{\omega_c}$ and the tunneling strength between cavity fields is $J \sim \omega_c$ [51]. Here, in order to satisfy the rotating wave approximation, we require ω_a/g_a, $\omega_c/g_a \gg |\Delta/g_a|$. This system includes N excitations [$N = \sum_i(a_i^\dagger a_i + \sigma_i^+\sigma_i^-) = \sum_i(n_i^c + n_i^a)$ is the total number of atomic and photonic excitations]. The filling factor is $\nu \equiv N/L = 1$, unless expressly specified otherwise. Actually, as the diagonalization of the generic Hamiltonian $H_{\rm gen}$ works in a fixed total number of excitation N with the rotating wave approximation, the properties of the system are related to the relative value between the atomic and the photonic frequencies, but not to their absolute value, then the rotating frame transformation can be used here to discuss the properties of the system. The JCH model has a reflection symmetry under the reflection (parity) operation P about the center of coupled-cavity arrays. Hilbert space can be decomposed into symmetric $p = 1$ and antisymmetric $p = -1$ subspaces. In the PBC, the JCH model also has translational symmetry and Hilbert space is further divided into subspaces with different quasimomentum Q. The general basis of full Hilbert space of H, with a space dimension

$$\mathcal{N} = \sum_{s=1}^{\min[N,L]} \left(L\frac{(N+L-s-1)!}{(N-s)!(L-s)!s!} \right) \tag{2.3}$$

is shown by the direct product of the cavity field states and atom states $|\mathbf{n}\rangle \equiv \prod_i |n_i, e(g)\rangle_i$. We mainly use numerical calculation in the irreducible Hilbert subspace $\mathcal{D} \approx \mathcal{N}/2L$ with $Q = 0$ and $p = -1$ for the PBC. When each on-site decouples, one only considers the interaction term $H_{\rm int}$ of the Hamiltonian and the effective local Jaynes-Cummings Hamiltonian can be easily diagonalized. One can obtain the eigenstates known as dressed states, $|\pm, n_i\rangle = [(\Delta/2 \pm \chi_{n_i})|n_i, g\rangle + g_a\sqrt{n_i}|n_i - 1, e\rangle]/\sqrt{2\chi_{n_i}^2 \mp \chi_{n_i}\Delta}$ in the ith cavity, and the corresponding eigenenergies are $E_i^\pm = \Delta/2 \pm \chi_{n_i}$, with $\chi_{n_i} = \sqrt{g_a^2 n_i + \Delta^2/4}$. The eigenvectors of the local interaction Hamiltonian $H_{\rm int}$ are $\prod_{i=1}^L |\pm, n_i\rangle$. The eigenvectors of the tunneling Hamiltonian $H_{\rm tun}$ are the delocalized plane-wave (standing-wave) modes with different wave vectors from the Fock states for PBC (hard-wall boundary condition). The interaction term and the tunneling term are integrable and

analytically solvable in the real and momentum spaces, respectively. When the scaled tunneling strength J/g_a is around 1, the competition between tunneling and interaction makes the JCH model be nonintegrable and show spectral chaos and ergodicity [38]. When $J/g_a \to 0\,(\infty)$, the JCH model exhibits integrability and nonergodicity.

III. ENERGY SPECTRUM PHASE TRANSITION AND THERMALIZATION BEHAVIOR

For characterizing the ergodicity of the JCH model from the eigenstates' structure, the conventional method is based on the multifractal complexity by using finite-size GFDs [52,53]

$$\widetilde{D}_q = \frac{1}{1-q}\log_{\mathcal{N}} R_q, \quad \text{with} \quad R_q = \sum_\alpha |\psi_\alpha|^{2q}, \quad q \in \mathbb{R}^+, \tag{3.1}$$

where ψ_α is the amplitude of eigenvectors in a given orthonormal basis $|\mathbf{n}\rangle$ of size $\mathcal{N}$. The scaling of R_q is generically described by $R_q \sim \mathcal{N}^{-(q-1)D_q}$ with $D_q \equiv \lim_{\mathcal{N}\to\infty} \widetilde{D}_q$ ($D_q \in [0,1]$). When $\widetilde{D}_{q\geqslant 1} = 0$, the state is localized in the considered basis. When $\widetilde{D}_q = 1$ for all q moments, the state is ergodic. Otherwise, the state is extended nonergodic (multifractal). In this paper we only study the case $q = 1$, 2, and ∞. By using the L'Hôpital's rule, we can get the dimension $\widetilde{D}_1 = -\sum_\alpha |\psi_\alpha|^2 \log_{\mathcal{N}} |\psi_\alpha|^2$, which is the information dimension and governs the scaling of the Shannon information entropy. D_2 is known as a measure of the state's "volume" and affects the inverse participation ratio of the eigenstate. As for $\widetilde{D}_\infty$, it is equal to $\lim_{q\to\infty} \log_{\mathcal{N}}[(\sum_\alpha |\psi_\alpha|^{2q})^{1/(q-1)}] \approx -\log_{\mathcal{N}}(|\psi_\alpha|^2_{\max[\alpha]})$, only the largest term $|\psi_\alpha|^2$ will contribute to the summation and $q/(q-1) \to 1$ in the limit $q \to \infty$, and determined by the maximum value of the intensities in a certain basis [54].

In this section we analyze the phase transition of the energy spectrum for the ergodic and nonergodic regimes for different Δ/g_a. Eigenenergy is scaled as $\epsilon \equiv (E - E_{\min})/(E_{\max} - E_{\min}) \in [0,1]$, where $E_{\min}$ and $E_{\max}$ are the minimum and maximum of the eigenenergies, respectively, then the eigenstates can be chosen around energy targets [55–57]. In the random matrix theory, the discrimination between ergodic and nonergodic regimes can depend on spectral statistics [36,58]. We can capture the statistical features of spectrum by the level spacing ratios [59,60] $r_n = \min(\delta_{n+1}/\delta_n, \delta_n/\delta_{n+1})$, where $\delta_n = E_{n+1} - E_n$ is the nth level spacing and the eigenenergies are arranged in an ascending order. When the system is ergodic, which is expressed as a Gaussian-orthogonal ensemble (GOE), random matrix and the average level spacing ratios show the Wigner-Dyson distribution ($\langle r\rangle_{\rm WD} \approx 0.5295$) [60]. Otherwise, the system is nonergodic, which is just like a classical integrable system and shows as Poisson distribution ($\langle r\rangle_P \approx 0.386$) [4]. Next, combining $\langle r\rangle$ and $\langle\widetilde{D}_1\rangle$, we can judge which phase of the system is shown under different parameters. Due to the facts that the fluctuations of GFDs are particularly sensitive to the ergodic behavior than the average GFDs, we also consider its variance $\mathrm{var}(\widetilde{D}_1)$ [61]. When the value of $\mathrm{var}(\widetilde{D}_1)$ changes with the extreme drop, the state undergoes a transition from nonergodic to ergodic. In order to elucidate the asymptotic behavior of the GFDs in an ergodic region, the numerical results of $\langle\widetilde{D}_1\rangle$ and $\mathrm{var}(\widetilde{D}_1)$ are compared against the GOE values for the random matrix theory (RMT), which provides wonderful analytical approximation [10,61],

$$\langle\widetilde{D}_1\rangle_{\rm GOE} = \frac{H_{\mathcal{D}/2} - 2 + \ln 4}{\ln \mathcal{D}}, \tag{3.2}$$

$$\mathrm{var}(\widetilde{D}_1)_{\rm GOE} = \frac{(3\pi^2 - 24)(\mathcal{D}+2) - 8}{2(\mathcal{D}+2)^2 \ln^2 \mathcal{D}} - \frac{\psi^{(1)}\left(2 + \frac{\mathcal{D}}{2}\right)}{\ln^2 \mathcal{D}}, \tag{3.3}$$

where $H_n = \sum_{k=1}^n \frac{1}{k}$ and $\psi^{(1)}$ expresses the first derivative of the digamma function [62].

We divide the interval [0,1] of ϵ variation into 100 bins of equal width. When the eigenvalues and eigenvectors fall into each bin, mean values ($\langle r\rangle$, $\langle\widetilde{D}_1\rangle$) and variances $\mathrm{var}(\widetilde{D}_1)$ as a function of J/g_a can be computed with various atom-photon detuning in Fig. 1. A quasisquare region of spectral chaos also can be identified with $\Delta/g_a = 0$, $0.02 \lesssim J/g_a \lesssim 0.2$ and $0.1 \lesssim \epsilon \lesssim 0.9$ in Figs. 1(a), 1(d) and 1(g), where $\langle r\rangle \approx 0.5295$, $\langle\widetilde{D}_1\rangle$ closes to 1, and $\mathrm{var}(\widetilde{D}_1)$ is a smaller value with several orders of magnitude. On the other hand, other regions of eigenenergy spectrum may be nonergodic and cannot be thermalized in the thermodynamic limit. One can find that these three physical quantities exhibit a symmetry about $\epsilon = 0.5$. The reason is that, under the chiral operator $\Gamma = \Pi_{j\in\mathrm{even}} e^{\pi i a_j^\dagger a_j} \Pi_{j\in\mathrm{odd}} \sigma_j^z$, the Hamiltonian Eq. (2.2) has a chiral symmetry ($\Gamma H \Gamma^\dagger = -H$) in the resonance $\Delta/g_a = 0$ for an even number of the lattice sites of the PBC [38]. Chiral symmetric Hamiltonian satisfies $H\Gamma|\psi_n\rangle = -\Gamma H|\psi_n\rangle = -\Gamma E_n|\psi_n\rangle = -E_n\Gamma|\psi_n\rangle$, which means the corresponding energy spectra are symmetric [63]. It turns out that the eigenenergies are symmetrical about the zero energy. Since the eigenenergies are scaled as ϵ, the level spacing ratios $\langle r\rangle$, which is the function of eigenenergies, is symmetrical about the scaled eigenenergies at $\epsilon = 0.5$. On the other hand, the eigenstate $|\Psi_n\rangle = \Sigma_i^{\mathcal{N}} \psi_i|n\rangle$ meets the condition $\langle\Psi_n|\Gamma^\dagger\Gamma|\Psi_n\rangle = \langle\Psi_n|\Psi_n\rangle = \Sigma_i^{\mathcal{N}}|\psi_i|^2$. In fact, according to the form of the Γ operator, the phase difference between the same basis of these two eigenstates are 0 or π. Those two eigenstates have the same GFDs $\widetilde{D}_1$. And because the eigenenergies of states $|\Psi_n\rangle$ and $\Gamma|\Psi_n\rangle$ are E_n and $-E_n$, their GFDs $\widetilde{D}_1$ are also symmetrical about the scaled eigenenergies at $\epsilon = 0.5$. Thus, $\langle\widetilde{D}_1\rangle$ and $\mathrm{var}(\widetilde{D}_1)$ are also symmetric about $\epsilon = 0.5$.

From the energy-resolved density plot of $\langle\widetilde{D}_1\rangle$, one can find that the eigenenergy spectra gradually form several energy bands with the increase of $|\Delta/g_a|$ at small scaled tunneling strength. The region of ergodic spectra fans out as $|\Delta/g_a|$ increases. The eigenenergy spectra no longer have the ergodic region for $|\Delta/g_a| = 10$. Moreover, The behaviors of $\langle\widetilde{D}_2\rangle$ and $\langle\widetilde{D}_\infty\rangle$ are similar to that of $\langle\widetilde{D}_1\rangle$, thus we do not discuss these two quantities in this section.

The eigenenergy average level spacings and eigenstate analyzed are required far from the edges of the spectrum for the applicability of RMT [3]. Therefore, the low-lying excited states and the states with the highest energies should be excluded and we only chose (middle one-third) a part of the intermediate energy spectrum, which can reflect the ergodicity

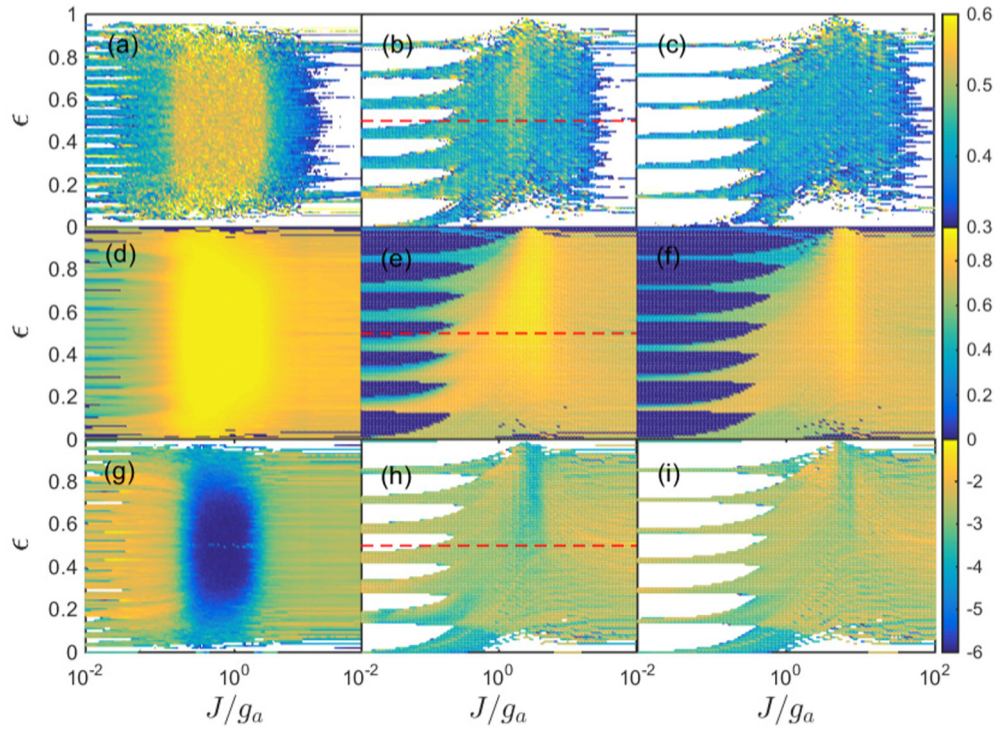

FIG. 1. The average level spacing ratios $\langle r\rangle$ (top), the average GFDs $\langle\widetilde{D}_1\rangle$ (middle), and the variance $\log[\mathrm{var}(\widetilde{D}_1)]$ (bottom) as functions of the scaled tunneling strength J/g_a and the scaled energy ϵ with $L = 8$, $\mathcal{D} = 9581$ for PBC. The first, second, and third column correspond to $|\Delta/g_a|$ equaling to 0, 5, and 10, respectively. Red dashed lines mark $\epsilon = 0.5$. The white area indicates that it goes beyond the display range of $\langle r\rangle$ and $\mathrm{var}(\widetilde{D}_1)$.

of the considered system. To clarify the influence of the size of Hilbert space on the eigenstates' structure and eigenenergies, we study the mean of $\langle r\rangle$ and $\langle\widetilde{D}_1\rangle$ and the $\mathrm{var}(\widetilde{D}_1)$ change with J/g_a and L for the detuning $|\Delta/g_a| = 0, 5, 10$ in Fig. 2. It should be noted that the value of detuning $|\Delta/g_a|$ is still far less than the atomic (photonic) frequency, i.e., $|\Delta/g_a| \ll \omega_a/g_a$ (ω_c/g_a) and satisfies the rotating wave approximation in this paper.

From Fig. 2(a) we can see that $\langle r\rangle$ is approximately the Wigner-Dyson distribution in the middle coupling strength J/g_a and $|\Delta/g_a| = 0$, and this feature is more obvious when the size L is large. Significantly, the average level spacing distributions of odd and even number of the lattice sites are different when the tunneling is large. This is because the lattice of the even length have chiral symmetry in the PBC, but the lattice of the odd length does not. For the case of the lattice of the odd length, both the first and the last sites are odd in the tunneling term, which prevents the Hamiltonian H from satisfying the chiral symmetry under the chiral operator Γ, and this effect is especially significant for large tunneling strength. It can be seen from the inset of Fig. 2(a) that under the hard-wall boundary condition (HWBC), both the odd and even number of the lattice sites have chiral symmetry, thus $\langle r\rangle$ is no difference. For $\langle\widetilde{D}_1\rangle$ [see Fig. 2(d)], when J/g_a is around 1, it exhibits a wider plateau for increasing size L and shows a extended nonergodic behavior, but the value of which depends on the size L. In addition, the corresponding $\mathrm{var}(\widetilde{D}_1)$ presents minimum value at intermediate range of J/g_a and rises sharply

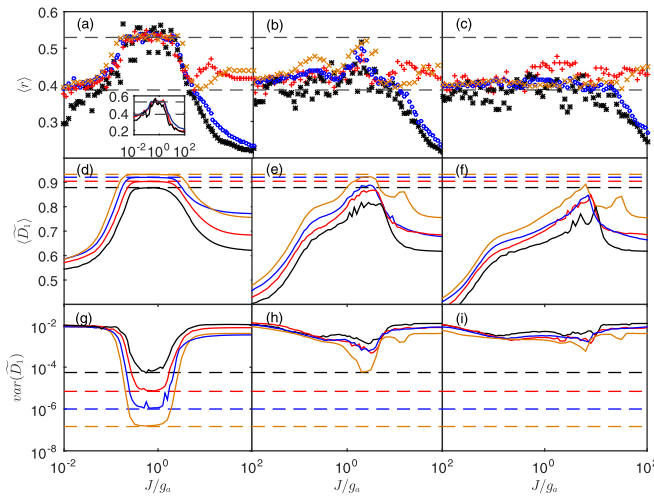

FIG. 2. The average level spacing ratios $\langle r\rangle$ (top), the average GFDs $\langle\widetilde{D}_1\rangle$ (middle), and the variance $\mathrm{var}(\widetilde{D}_1)$ (bottom) versus J/g_a at the middle one-third spectrum for different atom-photon detuning $|\Delta/g_a|$. Four colors represent four sizes $L = 6$ (black), 7 (red), 8 (blue), and 9 (yellow). The corresponding irreducible Hilbert subspaces are $\mathcal{D}_L = 399$, 1996, 9581, 47 692. Gray dashed lines represent $\langle r\rangle = 0.386$ and 0.5295 in (a)–(c). The inset in (a) is $\langle r\rangle$ for HWBC with $L = 5, 6, 7$. Dashed lines indicate the corresponding GOE value of $\langle\widetilde{D}_1\rangle$ and $\mathrm{var}(\widetilde{D}_1)$ in (d)–(f) and (g)–(i), respectively. The first, second, and third column correspond to $|\Delta/g_a| = 0$, 5, and 10, respectively.

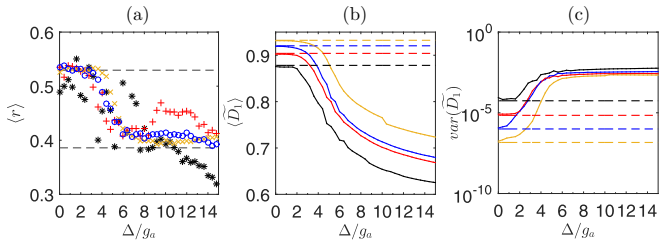

FIG. 3. (a) The average level spacing ratios $\langle r\rangle$, (b) the average GFDs $\langle \widetilde{D}_1\rangle$, and (c) the variance var$(\widetilde{D}_1)$ versus Δ/g_a at the middle one-third spectrum for the tunneling strength $J/g_a = 1$. Four colors represent four sizes $L = 6$ (black), 7 (red), 8 (blue), and 9 (yellow). Gray dashed lines represent $\langle r\rangle = 0.386$ and 0.5295 in (a)–(c). Dashed lines indicate the corresponding GOE value of $\langle \widetilde{D}_1\rangle$ and var$(\widetilde{D}_1)$ in (d)–(f) and (g)–(i), respectively.

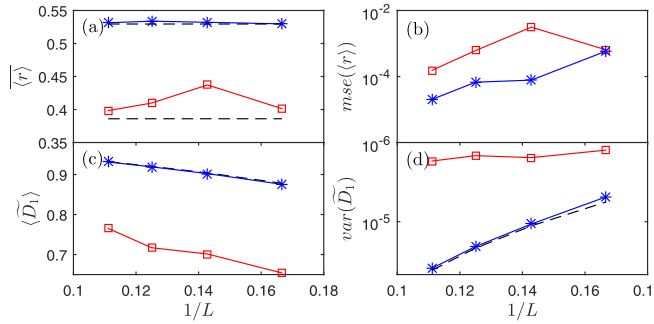

FIG. 4. The mean $\overline{\langle r\rangle}$ (a) and the mean squared error mse$(\langle r\rangle)$ (b) of the average level spacing ratios $\langle r\rangle$, the average GFDs $\langle \widetilde{D}_1\rangle$ (c), and the variance var$(\widetilde{D}_1)$ (d) versus $1/L$ for different atom-photon detuning $|\Delta/g_a| = 0$ (blue) and 10 (red). Black dashed lines represent $\langle r\rangle = 0.368$ and 0.5295 in (a). The black dashed lines indicate the corresponding GOE value of $\langle \widetilde{D}_1\rangle$ and var$(\widetilde{D}_1)$ in (c) and (d), respectively. The tunneling strength $J/g_a = 1$ for (c) and (d). The selected sizes are $L = 6, 7, 8, 9$.

on both sides of the valley in Fig. 2(g). It is noteworthy that the plateau values of $\langle \widetilde{D}_1\rangle$ and the valley of var$(\widetilde{D}_1)$ agree well with those expected value of Eqs. (3.2) and (3.3) for GOE eigenvectors, shown by dashed lines in Figs. 2(d) and 2(g). Obviously $\langle \widetilde{D}_1\rangle \to 1$, var$(\widetilde{D}_1) \to 0$, and $\langle r\rangle$ approaches 0.5295, when the size $L \to \infty$. At the other regions of the parameter J/g_a, we are not sure whether $\langle \widetilde{D}_1\rangle$ ($\langle r\rangle$) tends to zero (0.386) in the thermodynamic limit, but they mismatch the GOE of RMT and these regions are not an ergodic phase, which is similar to the Bose-Hubbard model [61]. Combining $\langle r\rangle$, $\langle \widetilde{D}_1\rangle$, and var$(\widetilde{D}_1)$, one knows that the intermediate region is standard ergodic phases and the regions on both sides are nonergodic phases with $|\Delta/g_a| = 0$ in the thermodynamic limit. However, with the increase of $|\Delta/g_a|$ (the second and third columns in Fig. 2), $\langle r\rangle$ of the original ergodic region is close to Poisson distribution with the increase of the size L. Meanwhile, the results of $\langle \widetilde{D}_1\rangle$ and var$(\widetilde{D}_1)$ are more and more inconsistent with the GOE of RMT and the ergodic region gradually disappears.

To know the transition from ergodic region to nonergodic region with the increase of atom-photon detuning more intuitively, the change of three physical quantities $\langle r\rangle$, $\langle \widetilde{D}_1\rangle$, and var$(\widetilde{D}_1)$ with Δ/g_a is drawn for $J/g_a = 1$ in Fig. 3. It can be found that when the detuning Δ/g_a is near zero, the standard ergodic behaviors are shown by three physical quantities. With the increase of detuning Δ/g_a, the system gradually deviates from the ergodic property and changes from the ergodic to nonergodic phase.

In detail, we also analyze the variation of four physical quantities $\overline{\langle r\rangle}$, mse$(\langle r\rangle)$, $\langle \widetilde{D}_1\rangle$, and var$(\widetilde{D}_1)$ versus size L for tunneling strength $J/g_a = 1$ and detuning $\Delta/g_a = 0$ (ergodic phase) and 10 (nonergodic phase) in Fig. 4, where $\overline{\langle r\rangle}$ is the mean of $\langle r\rangle$ for $J/g_a \in [0.4, 1]$ and mse$(\langle r\rangle) = \overline{\sum_i(\langle r\rangle_i - \langle r\rangle_{\rm pre})^2}$ is the corresponding mean squared error of average level spacing ratios $\langle r\rangle$, $\langle r\rangle_{\rm pre}$ is a predicted value which approaches 0.5295 for the ergodic phase and 0.386 for the nonergodic phase, respectively. The reason for this treatment of $\langle r\rangle$ is that it fluctuates relatively large in the finite size. From Fig. 4(a) one can find that $\overline{\langle r\rangle}$ of the ergodic phase ($\Delta/g_a = 0$) change with size L, which is in good agreement with the theoretical GOE values. For the nonergodic phase ($\Delta/g_a = 10$), $\overline{\langle r\rangle}$ has a trend close to the Poisson distribution with the increase of size L. In addition, the mean square error mse$(\langle r\rangle)$ of both phases decreases with the increase of size L in Fig. 4(b). In other words, with the increase of size L, the ergodic phase tends to Wigner-Dyson distribution, while the nonergodic phase tends to Poisson distribution. As for the average GFDs $\langle \widetilde{D}_1\rangle$ and the variance var$(\widetilde{D}_1)$ [see Figs. 4(c) and 4(d)], the physical quantities are in good agreement with the GOE values for the ergodic phase. The behaviors of $\langle \widetilde{D}_1\rangle$ and var$(\widetilde{D}_1)$ are a pronounced difference from the ones of GOE for the nonergodic phase, especially for var$(\widetilde{D}_1)$. Therefore, we predict that the phase transition occurs from ergodic to nonergodic cases with increasing atom-photon detuning in the thermodynamic limit. We all know that when J/g_a equals 0 or ∞, the eigenstates are massively degenerate. Thus, the density of states $\rho(\epsilon) = \Sigma_\alpha \delta(\epsilon - \epsilon_\alpha)/\mathcal{D}_L$ are shown in Fig. 5 to judge whether the average level spacing ratios of Poisson distribution for the large size is caused by energy level quasidegeneracy [27]. One can see that the density of states shows a series of spikes at $J/g_a = 0.01,\ 100$, and $|\Delta/g_a| = 0$ for a small system size L, but the structure gets diluted into a smooth continuum when increasing the system size. This tendency is also quite obvious at $J/g_a = 1$ and $|\Delta/g_a| = 10$.

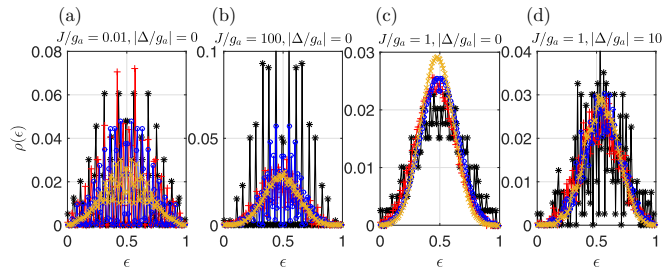

FIG. 5. Density of states $\rho(\epsilon)$ coarse-grained over the scaled energy ϵ for different J/g_a and atom-photon detuning $|\Delta/g_a|$. According to the number of eigenstates, ϵ is divided into 100 equal bins. The spikes mark the multiplet structure. Four colors and signal represent four sizes $L = 6$ (black star), 7 (red plus), 8 (blue circle), and 9 (yellow cross).

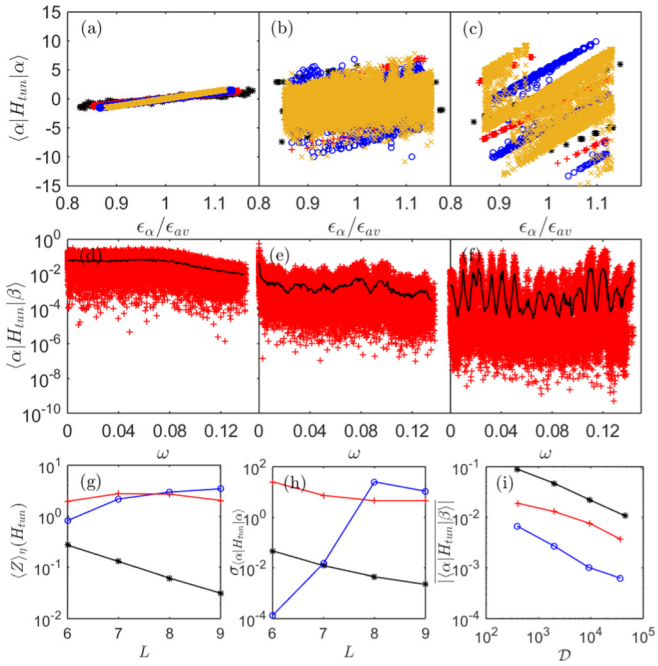

FIG. 6. The diagonal matrix elements of $H_{\rm tun}$ as a function of the rescaled energy for $|\Delta/g_a| = 0$ [(a)], 5 [(b)], 10 [(c)] with different sizes $L = 6$ (black star), 7 (red plus), 8 (blue circle), and 9 (yellow cross). The off-diagonal matrix elements of $H_{\rm tun}$ as a function of the rescaled energy for $|\Delta/g_a| = 0$ [(d)], 5 [(e)], 10 [(f)] for $L = 7$ (red plus). The corresponding black line is running averages with a subset length of 100. (g) The mean statistics of eigenstate-to-eigenstate fluctuations in Z_η vs the system size. (h) The variance $\sigma_{\langle\alpha|H_{\rm tun}|\alpha\rangle}$ vs the system size. (i) The average off-diagonal matrix elements $\overline{|\langle\alpha|H_{\rm tun}|\beta\rangle|}$ vs the irreducible Hilbert subspace $\mathcal{D}$. In (g)–(i), the black star, red plus, and blue circle lines correspond to $|\Delta/g_a| = 0$, 5, 10, respectively.

Moreover, the density of states is almost a smooth curve at $J/g_a = 1$ and $|\Delta/g_a| = 0$, even in the case of small system size, which is a Wigner-Dyson distribution and ergodic region. Therefore, the discussions of the ergodicity breaking in a small (large) J/g_a and $|\Delta/g_a|$ are independent of the spectrum in multiplets. Through analysis we find that one natural reason of the ergodicity breaking is the eigenenergies separation with the increase of the detuning $|\Delta/g_a|$.

In order to understand the thermalization properties of the ergodic and nonergodic phases, we further study whether the system obeys ETH for different $|\Delta/g_a|$. ETH is often used to describe the mechanism of the quantum thermalization in a generic quantum ergodic system [64,65]. When ETH ansatz is applicable, the diagonal matrix elements' fluctuation and the off-diagonal matrix elements of the observables are exponentially small with an increase of the system size [5,38,66–69]. In the following we focus on the middle one-third of eigenstates and verify whether the system meets the validity of the ETH for $J/g_a = 1$. The tunneling term $H_{\rm tun}$ is chosen, namely the photons kinetic energy, as a selected observable.

First, we study the diagonal part of the observable $\langle\alpha|H_{\rm tun}|\alpha\rangle$. Figures 6(a)–6(c) show the diagonal matrix elements of $H_{\rm tun}$ in the eigenstates $|\alpha\rangle$ of the irreducible Hilbert subspace as functions of $\epsilon_\alpha/\epsilon_{\rm av}$ for different $|\Delta/g_a|$, where ϵ_α is the corresponding scaled energy eigenvalue of the eigenstate $|\alpha\rangle$ and $\epsilon_{\rm av} = {\rm Tr}_{\mathcal{D}}\{(H - E_{\rm min})/(E_{\rm max} - E_{\rm min})\}$ is the average energy eigenvalue. The different colored symbols represent different system sizes. We find that the fluctuations of the eigenstate-expectation values decrease with size L in Figs. 6(a)–6(c) and eigenstate-expectation values become smooth functions of the energy density in the thermodynamic limit $L \to \infty$. However, when $|\Delta/g_a| = 10$, the fluctuation of the diagonal matrix element is generally invariant with the size increasing, which is in agreement with the behavior of the integrable system and dissatisfies the diagonal part of the ETH ansatz [70]. Furthermore, we quantitatively analyze the relation between the eigenstate-to-eigenstate fluctuations and the system's size L in the middle one-third spectrum. A measure of eigenstate-to-eigenstate fluctuations of diagonal expectation values is defined as $z_\alpha(H_{\rm tun}) = \langle\alpha + 1|H_{\rm tun}|\alpha + 1\rangle - \langle\alpha|H_{\rm tun}|\alpha\rangle$ [71]. In the middle one-third energy window, the mean can be given by

$$\langle Z\rangle(H_{\rm tun}) = \mathcal{D}^{-1} \sum_{|\alpha\rangle\in\mathcal{D}} |z_\alpha(H_{\rm tun})|. \tag{3.4}$$

The diagonal matrix element variance as a function of size L is also considered for the measure of ETH. The variance of diagonal expectation value around the microcanonical average is defined as

$$\sigma_{\langle\alpha|H_{\rm tun}|\alpha\rangle} = \frac{\Sigma_{\epsilon'_\alpha}(\langle\alpha|H_{\rm tun}|\alpha\rangle - \langle H_{\rm tun}\rangle_{\rm ME})^2}{N_{\rm state}}, \tag{3.5}$$

where $\epsilon'_\alpha \in [\epsilon_{\rm av} - \delta, \epsilon_{\rm av} + \delta]$, $N_{\rm state}$ is the number of ϵ'_α, $\langle H_{\rm tun}\rangle_{\rm ME} = \Sigma_{\epsilon'_\alpha}\langle\alpha|H_{\rm tun}|\alpha\rangle/N_{\rm state}$ is the microcanonical ensemble average, and δ (we choose $\delta = 0.05$) is a macroscopically small energy width [70,72]. From Fig. 6(g) one can see that the statistical average of eigenstate-to-eigenstate fluctuations $\langle Z\rangle_\alpha(H_{\rm tun})$ change with size L for different detuning $|\Delta/g_a|$. When $|\Delta/g_a| = 0$, the fluctuations exponentially decrease as the system size L increases. As the detuning $|\Delta/g_a|$ is relatively large, the fluctuations hardly decrease with size L. The behavior of the variance $\sigma_{\langle\alpha|H_{\rm tun}|\alpha\rangle}$ is similar to the that of $\langle Z\rangle_\alpha(H_{\rm tun})$ [see Fig. 6(h)], but the results in small size are not as expected for $|\Delta/g_a| = 10$.

We also briefly discuss the off-diagonal matrix elements $\langle\alpha|H_{\rm tun}|\beta\rangle$ of the tunneling operator to prove whether the off-diagonal part of the ETH ansatz is satisfied for different $|\Delta/g_a|$. The eigenstates are limited to a narrow energy window $(1 - \delta) < \bar{\epsilon}/\epsilon_{\rm av} < (1 + \delta)$ and $\bar{\epsilon} = (\epsilon_\alpha + \epsilon_\beta)/2$. The running average line becomes rougher with the increase of detuning and the overall fluctuation is larger in the nonergodic phase than the ergodic one for $\langle\alpha|H_{\rm tun}|\beta\rangle$ versus $\omega = \epsilon_\alpha - \epsilon_\beta$ in Figs. 6(d) and 6(e). But the average off-diagonal matrix elements of the tunneling operator $\overline{|\langle\alpha|H_{\rm tun}|\beta\rangle|}$ are exponentially small with different irreducible Hilbert subspaces $\mathcal{D}$ for different Δ/g_a in Fig. 6(i). Thus, the difference between ergodic and nonergodic phases is not obvious for the off-diagonal elements.

Therefore, the results in Fig. 6 reveal that the observable in the middle one-third spectrum obeys ETH for $|\Delta/g_a| = 0$ and violates of ETH for $|\Delta/g_a| = 10$.

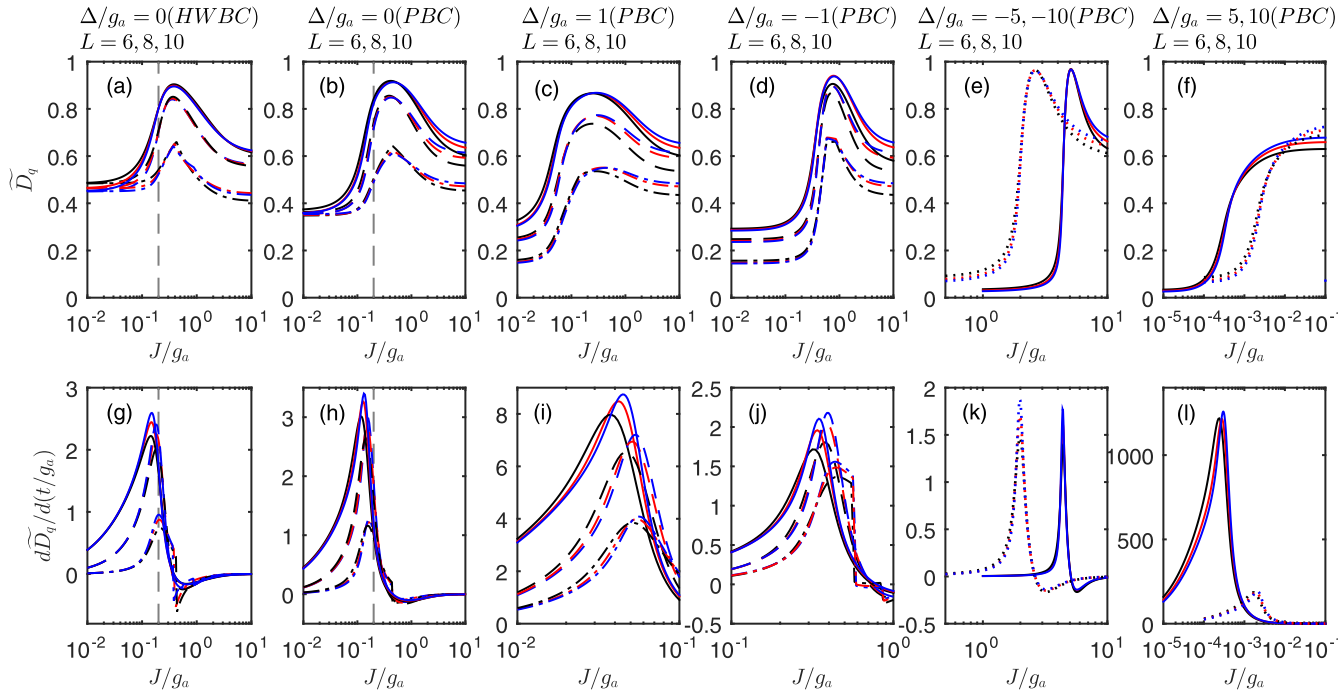

FIG. 7. The finite-size GFDs $\widetilde{D}_q$ (top) and its derivative $d\widetilde{D}_q/d(J/g_a)$ (bottom) as a function of the scaled tunneling strength J/g_a. We chose the basis of the product of the cavity field states and atom states $|\mathbf{n}\rangle$. From left to right, different subgraphs represent different conditions. Black, red, and blue lines correspond to the size L from small to large. The solid lines are $\widetilde{D}_1$, the dashed lines are $\widetilde{D}_2$, and the dot-dashed lines are $\widetilde{D}_\infty$ in the first four columns. The dotted (solid) line is the $\widetilde{D}_1$ for $|\Delta/g_a| = 5$ (10) in the last two columns. The vertical dotted line marks $J_c/g_a = 0.2$.

IV. THE ERGODICITY AND PHASE TRANSITION OF GROUND STATE

In this section we verify whether GFDs can determine the ground state phase transition and whether the SF and MI phases have a definite many-body multifractality. For integer filling factor ν and $J/g_a \to 0$, the ground state is given by $|\Psi(J/g_a = 0)\rangle = \prod_i |-, \nu\rangle_i$. Otherwise, when $J/g_a \to \infty$, we can only consider the tunneling term of the Hamiltonian H and the ground state is shown by the Fock basis of photons for PBC, $|\Psi(J/g_a = \infty)\rangle = \sum_i^{\mathcal{N}} \sqrt{\frac{N!}{L^N \nu_1!\nu_2!\ldots\nu_L!}} (\prod_j |\nu, g\rangle_j)_i$, which is similar to the results of the Bose-Hubbard model [53]. One can get GFDs analytically from the thermodynamic limit for $J/g_a = \infty$ ($D_1 = 0.941, D_2 = 0.907, D_\infty \approx 0.721$, for $\nu = 1$) [54,73]. In other words, the ground state shows multifractality in the Fock basis of photons, which is in an extended nonergodic phase. Through numerical analysis one can find that when J/g_a is extremely small, $\widetilde{D}_q$ of the ground state is equal to zero, which is a localized state. However, when J/g_a is extraordinarily large, the ground state is an extended nonergodic state with $0 < \widetilde{D}_q < 1$.

In the following we calculated numerically $\widetilde{D}_1$, $\widetilde{D}_2$, and $\widetilde{D}_\infty$ with J/g_a for different conditions. The gradient of $\widetilde{D}_q$ has its maximal value near the phase transition point in the finite size for the ground state MI-SF phase transition [53,54]. Therefore, in order to determine the ground state phase transition point, we also plot the derivative of $\widetilde{D}_q$ with J/g_a. In Fig. 7 we draw $\widetilde{D}_q$ and $d\widetilde{D}_q/d(J/g_a)$ with different Δ/g_a. The vertical dotted line in the subgraphs is the MI-SF phase transition critical point of the one-dimensional JCH model, i.e., $J_c/g_a \approx 0.2$ [74,75]. The value of $\widetilde{D}_q$ gets closer to a small value with $J/g_a \ll 1$ as the size L increases, which can be clearly obtained by finite-size analysis. At the large J/g_a, the value of $\widetilde{D}_q$ shows multifractal behavior and increases with the increasing of size L. On the other hand, through the derivative $d\widetilde{D}_q/d(J/g_a)$, we can better judge the phase transition critical point. From $d\widetilde{D}_q/d(J/g_a)$ versus J/g_a in Figs. 7(g)–7(j), one can find that the absolute value of the maximum derivative of $\widetilde{D}_q$ approaches the critical point with the increase of size L, which is independent of the boundary conditions. Under different boundary conditions, a slight distinction appears with the increase of size L, and $|d\widetilde{D}_q/d(J/g_a)|_{\max}$ may approach the phase transition critical point in another direction, especially for $\widetilde{D}_\infty$. Thus, $d\widetilde{D}_q/d(J/g_a)$ is a good quantity to judge the MI-SF phase transition.

Furthermore, we can determine the range of phase transition critical point J_c/g_a in the case of different filling factor ν and detuning Δ/g_a by two directions of the maximum value of $|d\widetilde{D}_q/d(J/g_a)|$ approaching the phase transition critical point under PBC and HWBC. For example, we find that for $\Delta/g_a = 1$, $J_c/g_a \in (0.06, 0.07)$, for $\Delta/g_a = -1$, $J_c/g_a \in (0.39, 0.45)$ in Figs. 7(i) and 7(j). Interestingly, the critical point t_c/g_a gradually moves to the right (left) with the increase (decrease) of Δ/g_a and $\widetilde{D}_q$ tends to zero with J/g_a close to zero in the finite size, as $|\Delta/g_a|$ gets bigger and bigger. In detail, we also found that $\widetilde{D}_q$ changes suddenly in a certain value J/g_a especially for $\widetilde{D}_\infty$, which makes $\widetilde{D}_q$ sometimes unsuitable for describing MI-SF phase transitions. The result of the mutation may be that we consider the subspace of the center-of-mass

quasimomentum $Q = 0$ in the translational symmetry. However, we find that, when $\Delta/g_a = -1$ or in HWBC, the change of $\widetilde{D}_\infty$ is discontinuous even in the whole Hilbert space. The another result is the inhomogeneous variation of the largest term $|\psi_\alpha|$ in the finite size. From Fig. 7 one can draw a conclusion that $\widetilde{D}_\infty$, as a function of J/g_a, is a smooth curve in the thermodynamic limit. What is particularly interesting is that the positive and negative signs of detuning have an opposite effect on the ground state phase transition, which is different from the results of the excited states. Through finite-size analysis, a strict ergodic SF phase may not emerge at any atom-photon detuning in the thermodynamic limit for the ground state, which should be further verified by an experiment of the 1D JCH system in the future.

V. CONCLUSION

In brief, using exact diagonalization, we have provided an integral picture of the ergodic and nonergodic phases of the one-dimensional JCH model for the excited state on the basis of $|\mathbf{n}\rangle$. Through the average level spacing ratios, the average GFDs and the GFDs' fluctuations, we can distinguish the ergodic and nonergodic phases. The ergodic phases of eigenvectors exist in the thermodynamic limit and are well described by RMT. The phase transition from a nonergodic to an ergodic phase occurs with the increase of the atom-photon detuning. We also find that the nonergodic phase closes to Poisson distribution and violates the ETH. As for the ground state, we describe the characteristics of many-body multifractality for different atom-photon detuning. The change rate of GFD can describe the MI-SF phase transition and the extended nonergodic MI (SF) phase can be achieved. We also find that the phase transition critical point can be identified easily in a very small range of parameters with large size and different boundary conditions, which reduces the dependence on complex numerical methods to study the superfluid-Mott-insulation phase transition.

ACKNOWLEDGMENTS

This work was supported by National Natural Science Foundation of China (Grants No. 11874190, and No. 12047501). Support was also provided by Supercomputing Center of Lanzhou University.

[1] A. M. Ozorio de Almeida, *Hamiltonian Systems: Chaos and Quantization* (Cambridge University Press, Cambridge, England, 1988).
[2] E. Ott, *Chaos in Dynamical Systems* (Cambridge University Press, Cambridge, England, 1993).
[3] L. D'Alessio, Y. Kafri, A. Polkovnikov, and M. Rigol, Adv. Phys. **65**, 239 (2016).
[4] M. V. Berry and M. Tabor, Proc. R. Soc. London Ser. A **356**, 375 (1977).
[5] J. M. Deutsch, Phys. Rev. A **43**, 2046 (1991).
[6] M. V. Berry, J. Phys. A: Math. Gen. **10**, 2083 (1977).
[7] D. Delande and J. C. Gay, Phys. Rev. Lett. **57**, 2006 (1986).
[8] I. M. Khaymovich, M. Haque, and P. A. McClarty, Phys. Rev. Lett. **122**, 070601 (2019).
[9] G. De Tomasi and I. M. Khaymovich, Phys. Rev. Lett. **124**, 200602 (2020).
[10] F. Haake, *Quantum Signatures of Chaos* (Springer, Berlin, 2006).
[11] B. V. Chirikov, in *Chaos and Quantum Mechanics*, Les Houches Lecture Series, edited by M.-J. Giannoni, A. Voros, and J. Zinn-Justin (Elsevier, Amsterdam, 1991), Vol. 52, pp. 443–545.
[12] E. B. Rozenbaum and V. Galitski, Phys. Rev. B **95**, 064303 (2017).
[13] C. Rylands, E. B. Rozenbaum, V. Galitski, and R. Konik, Phys. Rev. Lett. **124**, 155302 (2020).
[14] M. Fava, R. Fazio, and A. Russomanno, Phys. Rev. B **101**, 064302 (2020).
[15] S. Notarnicola, F. Iemini, D. Rossini, R. Fazio, A. Silva, and A. Russomanno, Phys. Rev. E **97**, 022202 (2018).
[16] B. L. Altshuler, Y. Gefen, A. Kamenev, and L. S. Levitov, Phys. Rev. Lett. **78**, 2803 (1997).
[17] I. V. Gornyi, A. D. Mirlin, and D. G. Polyakov, Phys. Rev. Lett. **95**, 206603 (2005).
[18] R. Nandkishore and D. A. Huse, Annu. Rev. Condens. Matter Phys. **6**, 15 (2015).
[19] J. Z. Imbrie, V. Ros, and A. Scardicchio, Annalen der Physik **529**, 1600278 (2017).
[20] D. A. Abanin, E. Altman, I. Bloch, and M. Serbyn, Rev. Mod. Phys. **91**, 021001 (2019).
[21] V. A. Yurovsky and M. Olshanii, Phys. Rev. Lett. **106**, 025303 (2011).
[22] A. Smith, J. Knolle, D. L. Kovrizhin, and R. Moessner, Phys. Rev. Lett. **118**, 266601 (2017).
[23] A. Smith, J. Knolle, R. Moessner, and D. L. Kovrizhin, Phys. Rev. Lett. **119**, 176601 (2017).
[24] M. Brenes, M. Dalmonte, M. Heyl, and A. Scardicchio, Phys. Rev. Lett. **120**, 030601 (2018).
[25] A. Smith, J. Knolle, R. Moessner, and D. L. Kovrizhin, Phys. Rev. Lett. **123**, 086602 (2019).
[26] A. Smith, J. Knolle, R. Moessner, and D. L. Kovrizhin, Phys. Rev. B **97**, 245137 (2018).
[27] A. Russomanno, S. Notarnicola, F. M. Surace, R. Fazio, M. Dalmonte, and M. Heyl, Phys. Rev. Research **2**, 012003(R) (2020).
[28] P. Karpov, R. Verdel, Y.-P. Huang, M. Schmitt, and M. Heyl, Phys. Rev. Lett. **126**, 130401 (2021).
[29] E. van Nieuwenburg, Y. Baum, and G. Refael, Proc. Natl. Acad. Sci. USA **116**, 9269 (2019).
[30] M. Schulz, C. A. Hooley, R. Moessner, and F. Pollmann, Phys. Rev. Lett. **122**, 040606 (2019).
[31] T. Prosen, Phys. Rev. Lett. **80**, 1808 (1998).
[32] T. Prosen, Phys. Rev. E **60**, 3949 (1999).
[33] W. Morong, F. Liu, P. Becker, K. S. Collins, L. Feng, A. Kyprianidis, G. Pagano, T. You, A. V. Gorshkov, and C. Monroe, Nature (London) **599**, 393 (2021).

[34] Q. Guo, C. Cheng, H. Li, S. Xu, P. Zhang, Z. Wang, C. Song, W. Liu, W. Ren, H. Dong, R. Mondaini, and H. Wang, Phys. Rev. Lett. **127**, 240502 (2021).

[35] M. Pino, L. B. Ioffe, and B. L. Altshuler, Proc. Natl. Acad. Sci. U.S.A. **536**, 113 (2016).

[36] A. Russomanno, M. Fava, and R. Fazio, Phys. Rev. B **102**, 144302 (2020).

[37] Q. Li, J.-L. Ma, T. Huang, L. Tan, H.-Q. Gu, and W.-M. Liu, Europhys. Lett. **134**, 20007 (2021).

[38] Q. Li, J.-L. Ma, and L. Tan, Phys. Scr. **96**, 125709 (2021).

[39] M. J. Werner and A. Imamoglu, Phys. Rev. A **61**, 011801(R) (1999).

[40] C.-Y. Chen, X.-L. Zhang, Z. J. Deng, K.-L. Gao, and M. Feng, Phys. Rev. A **74**, 032328 (2006).

[41] M. Aichhorn, M. Hohenadler, C. Tahan, and P. B. Littlewood, Phys. Rev. Lett. **100**, 216401 (2008).

[42] J.-G. Li, J. Zou, and B. Shao, Phys. Rev. A **81**, 062124 (2010).

[43] P. G. Di Stefano, E. Paladino, A. D'Arrigo, and G. Falci, Phys. Rev. B **91**, 224506 (2015).

[44] E. Sela, V. Fleurov, and V. A. Yurovsky, Phys. Rev. A **94**, 033848 (2016).

[45] A. D. Greentree, C. Tahan, J. H. Cole, and L. C. L. Hollenberg, Nat. Phys. **2**, 856 (2006).

[46] D. G. Angelakis, M. F. Santos, and S. Bose, Phys. Rev. A **76**, 031805(R) (2007).

[47] M. I. Makin, J. H. Cole, C. Tahan, L. C. L. Hollenberg, and A. D. Greentree, Phys. Rev. A **77**, 053819 (2008).

[48] M. J. Hartmann, F. G. S. L. Brandão, and M. B. Plenio, Laser Photonics Rev. **2**, 527 (2008).

[49] S. Schmidt and J. Koch, Annalen der Physik **525**, 395 (2013).

[50] C. Noh and D. G. Angelakis, Rep. Prog. Phys. **80**, 016401 (2017).

[51] X. Deng, C. Jia, and C.-C. Chien, Phys. Rev. B **91**, 054515 (2015).

[52] A. Rodriguez, L. J. Vasquez, K. Slevin, and R. A. Römer, Phys. Rev. B **84**, 134209 (2011).

[53] J. Lindinger, A. Buchleitner, and A. Rodríguez, Phys. Rev. Lett. **122**, 106603 (2019).

[54] J. Lindinger, Multifractal properties of the ground state of the Bose-Hubbard model, M.Sc. thesis, Albert-Ludwigs-Universität Freiburg, 2017.

[55] F. Pietracaprina, N. Macé, D. J. Luitz, and F. Alet, SciPost Phys. **5**, 045 (2018).

[56] S. Balay, S. Abhyankar, M. F. Adams, J. Brown, P. Brune, K. Buschelman, L. Dalcin, A. Dener, V. Eijkhout, W. D. Gropp, D. Karpeyev, D. Kaushik, M. G. Knepley, D. A. May, L. C. McInnes, R. T. Mills, T. Munson, K. Rupp, P. Sanan, B. F. Smith, S. Zampini, H. Zhang, and H. Zhang, PETSc Users Manual, Technical Report No. ANL-95/11- Revision 3.13 (Argonne National Laboratory, 2020).

[57] V. Hernandez, J. E. Roman, and V. Vidal, ACM Trans. Math. Softw. **31**, 351 (2005).

[58] M. L. Mehta, *Random Matrices* (Academic, Boston, 1991).

[59] V. Oganesyan and D. A. Huse, Phys. Rev. B **75**, 155111 (2007).

[60] Y. Y. Atas, E. Bogomolny, O. Giraud, and G. Roux, Phys. Rev. Lett. **110**, 084101 (2013).

[61] L. Pausch, E. G. Carnio, A. Rodríguez, and A. Buchleitner, Phys. Rev. Lett. **126**, 150601 (2021).

[62] F. W. J. Olver, A. B. Olde Daalhuis, D. W. Lozier, B. I. Schneider, R. F. Boisvert, C. W. Clark, B. R. Miller, B. V. Saunders, H. S. Cohl, and M. A. McClain, NIST Digital Library of Mathematical Functions, http://dlmf.nist.gov/, Release 1.0.27 of 2020-06-15.

[63] J. K. Asbóth, L. Oroszlány, and A. Pályi, *A Short Course on Topological Insulators* (Springer, Berlin, 2016).

[64] M. Srednicki, J. Phys. A: Math. Gen. **29**, L75 (1996).

[65] M. Srednicki, J. Phys. A: Math. Gen. **32**, 1163 (1999).

[66] M. Srednicki, Phys. Rev. E **50**, 888 (1994).

[67] M. Rigol, V. Dunjko, and M. Olshanii, Nature (London) **452**, 854 (2008).

[68] N. Linden, S. Popescu, A. J. Short, and A. Winter, Phys. Rev. E **79**, 061103 (2009).

[69] E. Khatami, G. Pupillo, M. Srednicki, and M. Rigol, Phys. Rev. Lett. **111**, 050403 (2013).

[70] W. Beugeling, R. Moessner, and M. Haque, Phys. Rev. E **89**, 042112 (2014).

[71] H. Kim, T. N. Ikeda, and D. A. Huse, Phys. Rev. E **90**, 052105 (2014).

[72] T. N. Ikeda, Y. Watanabe, and M. Ueda, Phys. Rev. E **87**, 012125 (2013).

[73] E. Bogomolny, Multifractality in simple systems (2012), presentation at the conference "Complex patterns in wave functions: Drums, graphs, and disorder" at the Kavli Royal Society Centre, UK.

[74] D. Rossini and R. Fazio, Phys. Rev. Lett. **99**, 186401 (2007).

[75] A. Mering, M. Fleischhauer, P. A. Ivanov, and K. Singer, Phys. Rev. A **80**, 053821 (2009).